THE JOURNAL OF BIOLOGICAL CHEMISTRY VOL. 282, NO. 21, pp. 15516–15527, May 25, 2007

Kinetic Analysis of the Entire RNA Amplification Process by Qβ Replicase*[S]

Received for publication, January 11, 2007, and in revised form, April 5, 2007 Published, JBC Papers in Press, April 5, 2007, DOI 10.1074/jbc.M700307200

Kazufumi Hosoda[‡], Tomoaki Matsuura[§], Hiroshi Kita[¶], Norikazu Ichihashi[¶], Koji Tsukada[§], and Tetsuya Yomo[‡¶‖1]

From the [‡]Graduate School of Frontier Biosciences, the [§]Department of Biotechnology, Graduate School of Engineering, and the [‖]Department of Bioinformatics Engineering, Graduate School of Information Science and Technology, Osaka University, Osaka 565-0871, Japan and the [¶]Complex Systems Biology Project, Exploratory Research for Advanced Technology, Japan Science and Technology Agency, Osaka 565-0871, Japan

The kinetics of the RNA replication reaction by Qβ replicase were investigated. Qβ replicase is an RNA-dependent RNA polymerase responsible for replicating the RNA genome of coliphage Qβ and plays a key role in the life cycle of the Qβ phage. Although the RNA replication reaction using this enzyme has long been studied, a kinetic model that can describe the entire RNA amplification process has yet to be determined. In this study, we propose a kinetic model that is able to account for the entire RNA amplification process. The key to our proposed kinetic model is the consideration of nonproductive binding (*i.e.* binding of an enzyme to the RNA where the enzyme cannot initiate the reaction). By considering nonproductive binding and the notable enzyme inactivation we observed, the previous observations that remained unresolved could also be explained. Moreover, based on the kinetic model and the experimental results, we determined rate and equilibrium constants using template RNAs of various lengths. The proposed model and the obtained constants provide important information both for understanding the basis of Qβ phage amplification and the applications using Qβ replicase.

Qβ replicase is an RNA-dependent RNA polymerase responsible for replicating the RNA genome of coliphage Qβ (1) that plays a key role in the life cycle of the Qβ phage (2, 3). This enzyme is a heterotetramer composed of a β subunit encoded on the phage genome and three host proteins: ribosomal protein S1, elongation factor Tu (EF-Tu), and Ts (EF-Ts) (4). The replication reaction proceeds first by binding of the enzyme to the 3′-end of single-stranded RNA (plus strand), and synthesizes its complementary single-stranded RNA (minus strand), which then becomes the template for synthesis of another plus strand (5). Not all RNAs can be amplified by the Qβ replicase. The requirements for amplifiable RNAs are known to be the presence of a poly(C) sequence at the 3′-end of the RNA (6, 7) and some unique secondary structural features (8), whereas these are not sufficient for designing amplifiable RNAs (9, 10). Using the replicase, RNA can be amplified exponentially from a single copy to 10^{12} copies in less than 30 min without the need for any oligonucleotide primer (*de novo* initiation) (3).

Qβ replicase has been recognized as a representative single-stranded RNA replicase and has been used for various purposes, such as to investigate the kinetics of single-stranded RNA replication (11) and nonhomologous RNA recombination (12) and to study various aspects of molecular evolution (13), hypercycle (14), and the origin of life (15). In addition, it has also been used as a tool for molecular biology (*e.g.* for the amplification of a particular RNA (16, 17), for virus detection (18), for RNA sequencing (19), and for introducing mutations (20)). Therefore, it is important to understand the basis of the replication reaction.

However, at present, there is no kinetic model to account for the entire RNA amplification process by Qβ replicase, whereas the requirements for amplifiable RNAs have been studied in detail. To date, the RNA amplification process has been segregated into individual steps, such as binding (21, 22) and double-stranded production (23, 24), which have been analyzed kinetically to determine the rate or equilibrium constants. On the other hand, kinetic models to explain the entire amplification process have been studied mainly by computer simulation (5, 11, 25), and these studies have not resolved the following three observations: (i) the replication of the phage genome RNA is somehow inhibited by the genomic RNA itself (26, 27), (ii) the reaction velocity decreases in the late phase of the reaction (5, 28), and (iii) the catalytic constant seems to differ between the earlier and later phases of the amplification process (5). The bases of these observations are still unclear. Moreover, kinetic studies have been carried out using only short template RNAs (about 200 nucleotides (nt)[2] in length). Furthermore, the kinetic constants, such as polymerization rate and Michaelis-Menten constant, have not been determined. The kinetics of Qβ replicase provide important information not only for understanding the basis of Qβ phage amplification but also for applications using Qβ replicase.

In this study, we performed kinetic analyses of the entire process of RNA amplification by Qβ replicase based on a simple kinetic model. The key in our proposed kinetic model is the

* This research was supported by "The 21st Century Center of Excellence Program" and "Special Coordination Funds for Promoting Science and Technology: Yuragi Project" of the Ministry of Education, Culture, Sports, Science, and Technology, Japan. The costs of publication of this article were defrayed in part by the payment of page charges. This article must therefore be hereby marked "*advertisement*" in accordance with 18 U.S.C. Section 1734 solely to indicate this fact.

[S] The on-line version of this article (available at http://www.jbc.org) contains template RNA sequences.

[1] To whom correspondence should be addressed: Dept. of Bioinformatics Engineering, Graduate School of Information Science and Technology, Osaka University, 2-1 Yamadaoka, Suita, Osaka 565-0871, Japan. Tel.: 81-6-6879-4171; Fax: 81-6-6879-7428; E-mail: yomo@ist.osaka-u.ac.jp.

[2] The abbreviations used are: nt, nucleotide(s); ROX, 5-carboxy-X-rhodamine.

consideration of nonproductive binding (*i.e.* binding of an enzyme to the RNA where the enzyme cannot initiate the reaction). Nonproductive binding will reduce the amount of enzyme for productive binding (*i.e.* binding to the appropriate position of the RNA for initiation of the reaction). Here, we used RNAs varying widely in length, and measured the replication reaction in real time with high accuracy using SYBR® Green II (29). Our model was able to account for all of the results of the entire amplification process and the previously unresolved observations. Moreover, we obtained the kinetic constants directly from the experiments. In addition, we found a notable inactivation pattern of the enzyme, which can be regulated by GDP as an accelerator of inactivation and NTPs as inhibitors of GDP-dependent inactivation. Finally, we discuss the important information obtained in this study both for understanding the basis of Qβ phage amplification and for applications using Qβ replicase.

EXPERIMENTAL PROCEDURES

Qβ Replicase—Qβ replicase was purified as described previously (30). After purification, the enzyme solution was dialyzed against the storage buffer (25 mM Tris-HCl, pH 7.8, 125 mM NaCl, 2.5 mM $MgCl_2$, 0.5 mM EDTA, 10 mM 2-mercaptoethanol, 50% (v/v) glycerol). SDS-PAGE showed the purified enzyme to be composed of EF-Tu, EF-Ts, and β subunit. The purified enzyme seemed to contain two different types of enzyme, as revealed by preincubation experiments: one with high and another with low thermostability. In this study, the enzyme solution was incubated at 37 °C for 10 min prior to carrying out the replication reaction, which removed the less stable fraction of the enzyme. The observation that the enzyme solution consists of enzymes with distinct thermostability was made with different batches of the S1-less enzyme, enzyme with S1 subunit (29), fusion enzyme (30), and commercially available enzyme (Epicenter, Madison, WI). It should be noted that the ratio between high and low thermostable enzymes was different among batches (data not shown); therefore, we worked with the enzyme from a single batch.

Plasmids—Plasmid pUC-MDV-LR (31), kindly provided by Dr. Inokuchi (Teikyo University), was used to produce MDV-poly RNA. The plasmid carries the sequence of MDV-poly RNA downstream of the T7 promoter sequence, a SmaI restriction site at the 3′-end of the MDV-poly sequence, and a BglII site within the MDV-poly RNA sequence for cloning (32). Plasmids for synthesis of MDV-T12, MDV-CAT, MDV-dBETA, and MDV-BETA RNAs were constructed by inserting the 27-base sequence (5′-GATCATTTTTTTTTTTTGTTTTTTTTA), chloramphenicol acetyltransferase gene, the Qβ replicase β subunit gene lacking the 1072-nt segment between the two StyI sites of the gene, and the complementary strand of the Qβ replicase β subunit gene, respectively, into the BglII sites of pUC-MDV-LR.

S222 RNA is a mutant of the complementary strand of MDV-1 RNA, which contains six mutations, three insertions, and two deletions. S130 RNA is a 130-nt fragment of the 5′ terminal part of S222 RNA containing two deletions, seven mutations, and the addition of CCA at its 3′ terminus. These two RNAs were isolated in our laboratory as a product of spontaneous RNA amplification (33), their sequences were inserted into the pUC19 vector (ATCC 37254) under the control of the T7 promoter, and an AlwI cleavage site was placed at the 3′-end. All sequences of the transcript RNAs are shown in the supplemental materials.

Preparation of Template RNAs —Template RNAs were prepared by *in vitro* transcription from a plasmid DNA linearized with AlwI (for S130 and S222 RNAs) or SmaI (for the other RNAs), using T7 RNA polymerase (Takara, Shiga, Japan) according to the manufacturer's instructions. Subsequently, the template DNA was digested with DNase I (GE Healthcare, Buckinghamshire, UK). RNA was purified with RNeasy mini (Qiagen, Tokyo, Japan) according to the manufacturer's instructions and eluted in distilled water. The RNA solution was heated at 70 °C for 2 min and placed at room temperature for more than 5 min before use.

Real Time Detection of the Replication Reaction—The replication reaction (20 μl) was carried out at 37 °C by adding template RNA and 1 μl of Qβ replicase to the reaction buffer (125 mM Tris-HCl, pH 7.8, 5 mM $MgCl_2$, 0.1 mg/ml bovine serum albumin, 1.25 mM each of ATP, GTP, CTP, and UTP, 500 nM (for ABI PRISM 7700 Sequence Detector) or 200 nM (for Mx3005P™ QPCR System) 5-carboxy-X-rhodamine (ROX) reference dye (Invitrogen), 1× concentration of SYBR® Green II (Invitrogen), 5 mg/ml Triton X-100). ROX was added as an internal marker to normalize the difference among the tubes.

For analysis of the exponential phase and the saturation point, the reactions were carried out at 37 °C for 15 min in the presence of various concentrations (12.5, 25, 50, 100, 200, or 400 nM) of the enzyme and 0.004 nM (for S130, S222, MDV-poly, and MDV-T12 RNA) or 0.4 nM (for MDV-CAT, MDV-dBETA, and MDV-BETA RNA) template RNA. For analysis of the linear phase, the reactions were monitored at 37 °C for 2 h in the presence of a 10 nM concentration of the enzyme and 100 nM (for S130 and S222 RNA), 200 nM (for MDV-poly and MDV-T12 RNA), or 60 nM (for MDV-CAT, MDV-dBETA, and MDV-BETA RNA) template RNA.

The reaction mixtures were monitored at 37°C using an ABI PRISM 7700 Sequence Detector (PE Applied Biosystems) for analysis of exponential phase and saturation point or an Mx3005P™ QPCR System (Stratagene) for analysis of the linear phase. The output fluorescence spectrum excited at 488 nm from ABI7700 was decomposed to the spectrum of SYBR® Green II and ROX by the least squares method. The ratio of the peak value of the spectrum of SYBR® Green II to that of ROX, obtained by spectral decomposition, was employed as the signal intensity. For monitoring by Mx3005P, the ratio of the value of fluorescence emission at 516 nm (excitation at 492 nm) to that at 610 nm (excitation at 585 nm) was employed as the signal intensity.

The RNA concentration in the reaction was quantified using a standard curve of known concentration of the RNA determined by the absorbance *versus* the signal intensity for both instruments. The data intervals of ABI7700 and Mx3005P were ~6 and 30 s, respectively. The ABI7700 has high sensitivity and accuracy but a narrow dynamic range, whereas the Mx3005P has low sensitivity and accuracy but a broad dynamic range.

Analysis of the Exponential Phase—When the enzyme is in excess to the RNA, RNA is amplified exponentially with the rate k_{obs}. Here, the reaction can be assumed to be a continuous stirred tank reactor steady-state reaction (11), which is an assumption that the concentrations of all components in the reactor increase autocatalytically at the same rate, and the concentrations of Rt, *E*-Rp, and *E*-Rn (total RNA, enzyme bound to productive binding site of the RNA, and enzyme bound to nonproductive binding site of the RNA, respectively) can be written as follows.

$$\frac{d[Rt]}{dt}\cdot\frac{1}{[Rt]} = \frac{d[E\text{-Rp}]}{dt}\cdot\frac{1}{[E\text{-Rp}]} = \frac{d[E\text{-Rn}]}{dt}\cdot\frac{1}{[E\text{-Rn}]} = k_{obs} \quad \text{(Eq. 1)}$$

The rate equation for [Rt] and [*E*-Rp] in our model (Scheme 1) can be written as follows,

$$\frac{d[Rt]}{dt} = k_{cat}[E\text{-Rp}] \quad \text{(Eq. 2)}$$

$$\frac{d[E\text{-Rp}]}{dt} = k_1[E][Rp] - (k_{-1} + k_{cat})[E\text{-Rp}] \quad \text{(Eq. 3)}$$

where *E* represents free enzyme (*i.e.* $[E] = [Et] - [E\text{-Rp}] - [E\text{-Rn}]$, *Et* is total active enzyme), Rp is free productive binding sites of the RNA, k_1 and k_{-1} are the association and dissociation rates between the enzyme and productive binding site of the RNA, respectively, and k_{cat} is the catalytic rate constant. When $[E] \approx [Et]$ (which is the case at exponential phase), k_{obs} can be solved from Equations 1, 2, and 3 as follows.

$$k_{obs} = \frac{2k_{cat}[Et]}{\frac{k_{-1}+k_{cat}}{k_1} + [Et] + \sqrt{4[Et]\frac{k_{cat}}{k_1} + \left([Et] + \frac{k_{-1}+k_{cat}}{k_1}\right)^2}} \quad \text{(Eq. 4)}$$

We assumed $k_{-1} \gg k_{cat}$ or $k_{-1} \ll k_{cat}$ to reduce the parameter for fitting as follows. When k_{-1} is $\gg k_{cat}$ and k_{-1} is $\ll k_{cat}$, we obtained the following, respectively,

$$k_{obs} = \frac{k_{cat}[E_{280}]}{[E_{280}] + K_m/\alpha} \quad \text{(Eq. 5)}$$

and

$$k_{obs} = \frac{2k_{cat}[E_{280}]}{K_m/\alpha + [E_{280}] + \sqrt{4[E_{280}]K_m/\alpha + ([E_{280}] + K_m/\alpha)^2}} \quad \text{(Eq. 6)}$$

where K_m is $(k_{-1} + k_{cat})/k_1$ and $[E_{280}]$ is the enzyme concentration determined from the absorbance at 280 nm. α is the fraction of active enzyme ($[Et]$) in $[E_{280}]$ (*i.e.* $\alpha = [Et]/[E_{280}]$), which was found to differ significantly among batches of the enzyme preparation (data not shown). Therefore, we worked with enzyme from a single batch in this study. Both Equations 5 and 6 can give the values of k_{cat} and K_m; however, by computational simulation, k_{cat} was found to be estimated accurately regardless of the relation between k_{cat} and k_{-1}, and K_m was found with a difference of at most 50%.

Analysis of the Saturation Point—The saturation point is the end of the exponential phase, and we used the same assumption as the exponential phase that the reaction is at continuous stirred tank reactor steady state (as described above; see Equation 1). The rate equation for [*E*-Rn] in our model can be written as follows,

$$\frac{d[E\text{-Rn}]}{dt} = k_2[E][Rn] - k_{-2}[E\text{-Rn}] - k_{cat}[E\text{-Rn}]\frac{[E\text{-Rp}]}{[Rt]} \quad \text{(Eq. 7)}$$

where Rn is free nonproductive binding sites of the RNA ($[Rn] = n\cdot[Rt] - [E\text{-Rn}]$, where n is the number of nonproductive binding sites on a single RNA), and k_2 and k_{-2} are the association and dissociation rates between the enzyme and nonproductive binding sites of the RNA, respectively. The third term of Equation 7 represents the dissociation of *E*-Rn caused by the interaction with the elongating enzyme on the same template RNA. As in the exponential phase, we assumed $[E] \approx [Et]$. To reduce the parameter, we also assumed $[E\text{-Rp}] \approx [Rt]$, which can then be used to convert Equation 7 to the following,

$$[E\text{-Rn}] = \frac{n[Et][Rt]}{K_{m2} + [Et]} \quad \text{(Eq. 8)}$$

where K_{m2} is $(k_{-2} + 2k_{cat})/k_2$. At the saturation point ($[Rt] = [R_{sat}]$), the enzyme can be assumed to be saturated by binding to either the productive or the nonproductive binding site of RNA (*i.e.* $[Et] \approx [E\text{-Rp}] + [E\text{-Rn}]$) (11, 23), and we then obtained the following.

$$\frac{[R_{sat}]}{[E_{280}]} = \alpha\cdot\frac{K_{m2}/\alpha + [E_{280}]}{K_{m2}/\alpha + (n+1)[E_{280}]} \quad \text{(Eq. 9)}$$

The assumption that the enzyme is in excess to RNA ($[E] \approx [Et]$) is in conflict with the assumption that the enzyme is saturated with RNA ($[Et] \approx [E\text{-Rp}] + [E\text{-Rn}]$). Nevertheless, the values of n and K_{m2} can be determined by fitting the data using Equation 9 with high accuracy as described below. $[R_{sat}]$ was determined by fitting the time course of [Rt] to the following equation,

$$\ln[Rt] = \text{Boole}[t < t_{sat}]\cdot(k(t - t_{sat}) + \ln(at_{sat} + b)) + \text{Boole}[t_{sat} \le t]\cdot\ln(at + b) \quad \text{(Eq. 10)}$$

using Mathematica (Wolfram Research, Inc.), where a, b, k, and t_{sat} are the fitting parameters. t_{sat} is the reaction time at the saturation point. The Boole function (Boole[ϕ]) is also called Iverson's convention (34), which yields 1 if ϕ is true and 0 if ϕ is false. Therefore, the total RNA concentration ([Rt]) in Equation 10 increases exponentially over time when $t < t_{sat}$ and increases linearly over time when $t_{sat} < t$. The reaction times used to obtain $[R_{sat}]$ were 2–4, 2–5, 3–7, 3–7, 2–6, 3–7, and 2–9 min for S130, S222, MDV-poly, MDV-T12, MDV-CAT, MDV-dBETA, and MDV-BETA, respectively.

To test the fitting accuracy, we simulated the reaction based on the reaction scheme (Scheme 1) with various values of constants, including n and K_{m2}, with the enzyme concentrations used in the experiment and then estimated $[R_{sat}]$ values using the Boole function. In all cases, as with the experimental results

(Fig. 3*A*), the relationship between $[R_{sat}]/[E_{280}]$, and $[E_{280}]$ obeyed Equation 9. When we then fitted the results of the simulation using Equation 9, the values of both n and K_{m2} could be determined with at most 50% error, which justified our strategy of estimating these values.

Analysis of the Linear Phase—In the reaction initiated immediately from the linear phase, it can be assumed that the RNA is present in excess relative to the enzyme (*i.e.* [Rp] ≈ [Rt] and [Rn] ≈ n·[Rt]). First, we assumed that the association of productive binding is much faster than that of nonproductive binding (*i.e.* $k_1 \gg n \cdot k_2$), and the productive binding, including the catalytic process (*i.e.* $E + \mathrm{Rp} \rightleftharpoons E\text{-Rp} \rightarrow E + 2\mathrm{R}_{free}$ in Scheme 1), can be described as steady-state. Based on the assumptions, [*E*-Rp] can be written as follows.

$$[E\text{-Rp}] = \frac{([Et] - [E\text{-Rn}])[Rt]}{K_m + [Rt]} \qquad \text{(Eq. 11)}$$

Then we assumed that only a single molecule of enzyme can bind to each molecule of template RNA because the RNA is present in excess relative to the enzyme. In this case, the dissociation of *E*-Rn caused by the interaction with the elongating enzyme (the third term in Equation 7) is negligible. Based on this assumption, the rate equation for [*E*-Rn] can be described as follows.

$$\frac{d[E\text{-Rn}]}{dt} = k_2[E]n[Rt] - k_{-2}[E\text{-Rn}] \qquad \text{(Eq. 12)}$$

From Equations 11 and 12, and by assuming [Rt] ≫ K_m, we obtained the reaction velocity at time t without consideration of the enzyme inactivation ($V_{cor}(t)$) as follows,

$$V_{cor}(t) = \frac{k_{cat}[Et]\left(e^{-(k_{-2} + nk_2K_m)t} + \frac{K_i}{nK_m}\right)}{1 + \frac{K_i}{nK_m}} \qquad \text{(Eq. 13)}$$

where K_i is k_{-2}/k_2. In consideration of the enzyme inactivation (*i.e.* $[Et(t)] = [Et(0)] \cdot \exp(-k_{inact} \cdot t)$, k_{inact} is the rate of enzyme inactivation, and $Et(t)$ is the total active enzyme at reaction time t), we obtained the reaction velocity at time t ($V(t)$) as follows.

$$V(t) = \frac{k_{cat}\alpha[E_{280}]\left(e^{-(k_{-2} + nk_2K_m)\cdot t} + \frac{K_i}{nK_m}\right)}{1 + \frac{K_i}{nK_m}} \cdot e^{-k_{inact}\cdot t} \qquad \text{(Eq. 14)}$$

Equation 14 could not provide good fits for RNAs except S130 and S222 for two reasons. First, the initial enzyme concentration is much less than that of the initial RNA. This results in less of an increase in the signal intensity (*i.e.* lower velocity), in particular for RNAs amplified at low efficiency. Therefore, the error becomes larger relative to the increase in the signal. Second, the spontaneous RNA (33) emerges in the middle of the reaction and precludes homogeneous RNA amplification, particularly for RNAs amplified at low efficiency. Therefore, the real time data are plausible only until the emergence of the spontaneous RNA. It should be noted that the emergence of the spontaneous RNA could be detected not only by gel electrophoresis but also by real time measurement as a marked increase in signal intensity (velocity). We determined the values of $V_{cor}(0)$ and $V_{cor}(\infty)$ as the mean value of $V_{cor}(t)$ for the reaction time of 2–10 min and as the minimum value of $V_{cor}(t)$ averaged for 15 min, respectively. Since the occurrence of spontaneous RNA induced a sudden increase in the reaction velocity, we used the minimum value as $V_{cor}(\infty)$.

Enzyme Inactivation—The enzyme was incubated at 37 °C for various times under the buffer conditions described under "Results" and subsequently placed on ice for 5 min. Then the lacking NTPs were added, and the mixture was incubated at 37 °C to start the reaction. The fraction of the active enzyme was obtained as the ratio of the initial velocity after preincubation to the initial velocity without preincubation. The inactivation rate was determined by fitting the time course of the enzyme inactivation to a single exponential curve. The values of $K_{i(NTP)}$ were determined using the equation, $K_{i(NTP)} = [I_t]\ k_{inact\_inh}/(k_{inact\_MAX} - k_{inact\_inh})$, where k_{inact_MAX} and k_{inact_inh} are the inactivation rate in the presence of 1.25 mM GDP without and with NTPs, respectively, and $[I_t]$ is the total concentration of NTPs.

RESULTS

Real Time Measurement and the Two Phases of the RNA Amplification Process—Qβ replicase can amplify RNA exponentially starting from a small number of copies of the template RNA. In this study, RNA amplification was measured in real time using the fluorescent intercalating dye SYBR® Green II (29), as opposed to gel electrophoresis used mainly in previous studies, and this enabled us to perform detailed kinetic analysis. Fig. 1 shows a typical result of RNA amplification detected by real time measurement. The time courses of changes in RNA concentration and the reaction velocity are shown as *closed* and *open circles*, respectively. The velocity was determined from the slope of the RNA amplification curve. We confirmed that SYBR® Green II does not affect the replication reaction and that the lag time of fluorescence and photobleaching of the fluorescence were negligible by gel electrophoresis (data not shown).

The RNA amplification process can be decomposed into two phases (*i.e.* the exponential and linear phases) (5, 23). Fig. 1 shows the two phases: a steep increase in velocity, which corresponds to the exponential phase (about the first 3 min), and a decrease in velocity, which corresponds to the linear phase. We refer to the transition point of these two phases as the saturation point (around 3 min). The exponential phase is observed when the enzyme is present in excess relative to the RNA in molar ratio. Under such conditions, the RNA is amplified exponentially over time, because the RNA itself, which increases over time, is rate-limiting (*i.e.* it is autocatalytic). The linear phase is observed after the amplified RNA copy number reaches that of the working enzyme. Under such conditions, the RNA is amplified linearly over time, because the enzyme, which does not increase (but can decrease by inactivation or competitive inhibition as described later) over time, is rate-limiting. At the transition point from the exponential phase to the linear phase, the enzyme is saturated by the RNA (and *vice versa*), and

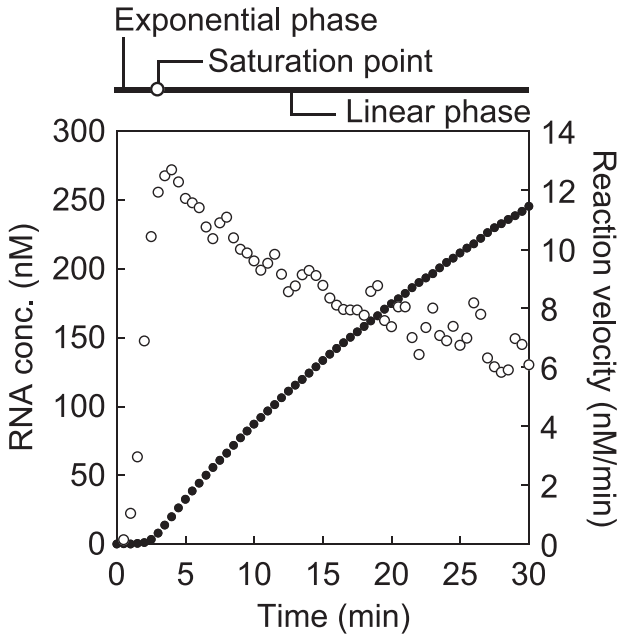

FIGURE 1. **Representative results of replication reaction by Qβ replicase measured in real time.** The reaction was initiated with 0.1 nM S222 RNA and the enzyme at 20 nM, and the time course of changes in the RNA concentration (*left axis*, ●) and the reaction velocity obtained as the slope for 1 min (*right axis*, ○) were plotted. The exponential and linear phases and the saturation point are depicted at the *top*.

we thus refer to this transition point as the saturation point. In this study, we analyzed the reaction individually for each phase: exponential phase, saturation point, and linear phase.

Proposal of a Kinetic Model—We proposed a simple kinetic model based on previous reports to determine the kinetic constants directly from the experiments. The presence of a poly(C) sequence at the 3′-end of the RNA (6, 7) and unique secondary structures at both 3′- and 5′-ends (8) are known to be necessary for amplifiable RNAs. Here, binding of the enzyme to such template RNA at an appropriate location where the replication reaction can be initiated is interpreted as productive binding. On the other hand, Qβ replicase is known to bind various RNAs, regardless of whether the RNA is amplifiable or not (22). Moreover, it has been reported that replication of the phage genome RNA is somehow inhibited by itself (26, 27). We also observed that a 30-base oligo-RNA, which is not amplifiable, competitively inhibited the replication reaction (not shown). These observations led us to propose the following: in addition to productive binding, Qβ replicase binds to RNA nonproductively, even to positions other than the productive binding sites of the amplifiable RNA, and such nonproductive binding may reduce the working enzyme concentration. Note that such competitive inhibition by nonproductive binding is also known for other enzymes (35), especially those that use polymers as substrates (36–38). Therefore, we proposed the kinetic model as follows,

$$E\text{-Rn} \underset{k_2\text{Rn}}{\overset{k_{-2}}{\rightleftharpoons}} E \underset{k_{-1}}{\overset{k_1\text{Rp}}{\rightleftharpoons}} E\text{-Rp} \xrightarrow{k_{cat}} E + 2\text{R}_{free}$$

SCHEME 1

where E represents free enzyme, R_{free} is free template RNA, Rp is free productive binding sites of the RNA ([Rp] = [Rt] − [E-Rp], where Rt is the total RNA), E-Rp is the enzyme bound to productive binding site of the RNA, Rn is free nonproductive binding sites of the RNA ([Rn] = n·[Rt] − [E-Rn], where n is the number of nonproductive binding sites on a single RNA), E-Rn is the enzyme bound to nonproductive binding sites of the RNA, k_1 and k_{-1} are the association and dissociation rates between the enzyme and productive binding site of the RNA, respectively, k_2 and k_{-2} are the association and dissociation rates between the enzyme and nonproductive binding sites of the RNA, respectively, and k_{cat} is the catalytic rate constant.

The unique feature of this model is the competitive inhibition of the enzyme by nonproductive binding to the template RNA. We assumed that enzyme bound to nonproductive binding sites does not inhibit elongation of the enzyme bound to the productive binding site of the same template RNA and does not affect the k_{cat} value, which is justified by the experimental data (described under "Discussion"). In this study, we determined the kinetic parameters directly from the experimental results based on this simple model and verified the validity of the model.

Analysis of the Exponential Phase—Exponential phase was analyzed to obtain k_{cat} and K_m ($= (k_{-1} + k_{cat})/k_1$) values. During the exponential phase, the enzyme is present in excess relative to the template RNA, and nonproductive binding (E-Rn ⇌ E) is negligible. Therefore, the reaction can be interpreted as a simple Michaelis-Menten-like model (*i.e.* E + Rp ⇌ E-Rp → $E + 2\text{R}_{free}$ in Scheme 1), and indeed this was the case (Fig. 2*B*). In the exponential phase, total RNA concentration ([Rt]) can be written as a function of the reaction time t, [Rt] = $[\text{Rt}_0]\cdot\exp(k_{obs}\cdot t)$, where $[\text{Rt}_0]$ is the initial concentration of the RNA, and k_{obs} is the observed rate of exponential amplification. We measured the reactions at the exponential phase using various concentrations of enzyme and seven different template RNAs differing in length from 130 to 2085 nt (Table 1). All seven sequences were derivatives of MDV-1 RNA, which is known to be an amplifiable RNA of Qβ replicase (39). More information on the sequences of these RNAs is given under "Experimental Procedures." Fig. 2*A* shows representative results of the time course of RNA amplification using S222 RNA as a template with a fixed concentration of RNA and different enzyme concentrations. In Fig. 2*B*, the rates of exponential amplification (k_{obs}; the slope in natural logarithm in Fig. 2*A*) for the seven different template RNAs are plotted against $[E_{280}]$, which are the enzyme concentrations determined from the absorbance at 280 nm. The total concentration of active enzyme ([Et]) is defined as $\alpha\cdot[E_{280}]$. α is the fraction of active enzyme, which can be determined experimentally by analysis of the saturation point (see below) (Fig. 3*A*).

During the exponential phase, k_{obs} can be approximated, depending on the values of k_{cat} and k_{-1}. When k_{-1} is $\gg k_{cat}$ and when k_{-1} is $\ll k_{cat}$, k_{obs} can be written as Equation 5 and 6, respectively (see "Experimental Procedures"). K_m is $(k_{-1} + k_{cat})/k_1$, which is the Michaelis-Menten constant between the enzyme and the productive binding site of the template RNA. Since we have no means to determine whether k_{-1} is $\gg k_{cat}$ or k_{-1} is $\ll k_{cat}$, we estimated k_{cat} and K_m/α values by fitting the

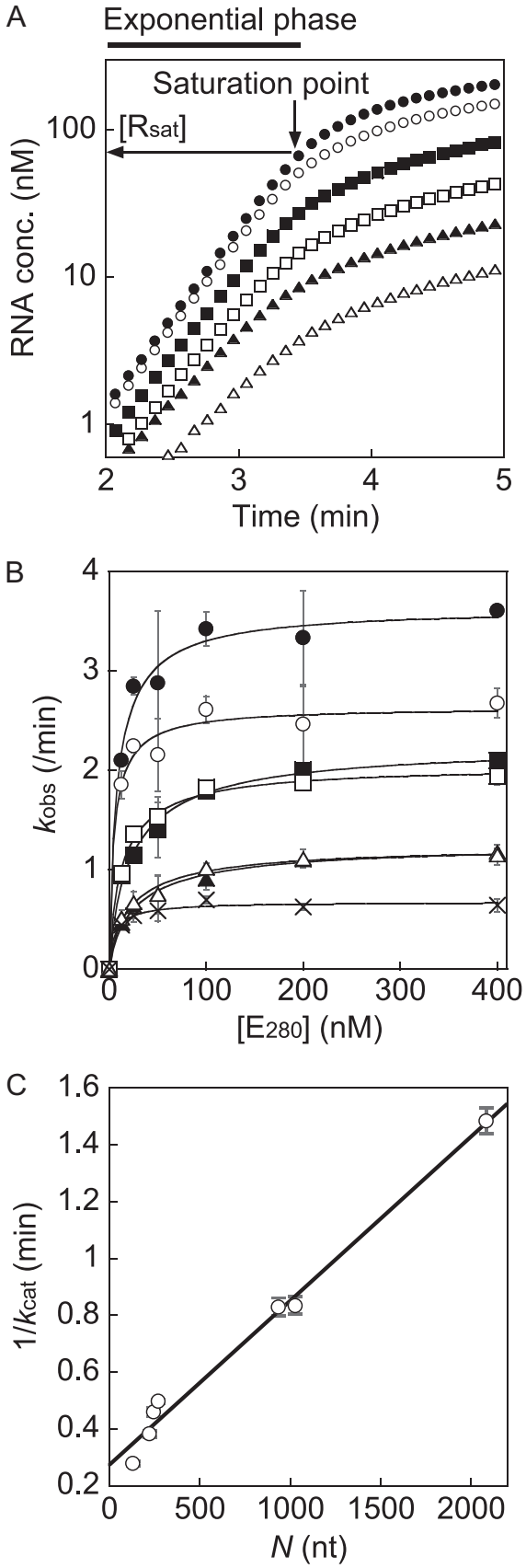

FIGURE 2. **Analysis of the exponential phase.** *A*, representative results of the time course of the replication reaction using 0.004 nM S222 RNA and the enzyme at 400 (●), 200 (○), 100 (■), 50 (□), 25 (▲), or 12.5 (△) nM. The exponential phase, the saturation point, and the RNA concentration at the saturation point ([R_{sat}]) for the reaction using 400 nM enzyme are shown. *B*, the observed rate of exponential amplification (k_{obs}) as a function of [E_{280}] for the following seven RNAs: S130 (●), S222 (○), MDV-poly (■), MDV-T12 (□), MDV-CAT (▲), MDV-dBETA (△), and MDV-BETA (×). The *solid lines* represent the fit of the data to Equation 5, which gave the k_{cat} and K_m/α values shown in Table 1. *C*, the correlation between $1/k_{cat}$ and *N*. The *solid line* represents the linear regression of the data that gave the k_{pol} and k_{others} values as described under "Results."

data to both Equations 5 and 6. When the values obtained from Equation 6 were compared with those obtained by Equation 5, k_{cat} was 2% larger and K_m was 30% smaller for all seven RNAs, and thus the differences were not significant. The values obtained with Equation 5 are shown in Table 1, but it should be noted that the k_{cat} values are plausible, and K_m may be overestimated but by at most 30%.

The inverse of k_{cat} can be considered as the time costs for the single catalytic reaction and can be written as $1/k_{cat} = N/k_{pol} + 1/k_{others}$, where k_{pol}, k_{others}, and N are the rate constant of polymerization for one nucleotide, rate constant of reactions other than polymerization (*i.e.* initiation and termination), and the nucleotide length of the template RNA, respectively. We found that $1/k_{cat}$ was proportional to N, and $k_{pol} = 28.9$/s and $k_{others} = 0.061$/s were determined from the slope and the intercept of the linear fit in Fig. 2*C*, respectively. It should be noted that the linearity observed in Fig. 2*C* suggests that the major differences in k_{cat} among the RNAs can be accounted for by the RNA length N alone.

It has been reported previously that RNAs of the same length can exhibit different catalytic rates depending on their sequence and structure (24, 40). Indeed, we observed that k_{cat} values were different among RNAs of similar lengths (*i.e.* S222, MDV-poly, and MDV-T12; see Table 1), which cannot be explained solely by the differences in their length. Nevertheless, the correlation observed in Fig. 2*C* suggests that the contributions of sequence and structure to the k_{cat} value are smaller than those of the length of the RNA, particularly when the RNA length varies widely. We were thus able to identify the relationship between k_{cat} and N and obtained values of k_{pol} and k_{others}. The value of k_{pol} (28.9/s) was comparable with those of other polymerases, including T7 polymerase (41), 3D polymerase (42), human immunodeficiency virus reverse transcriptase (43), RNA polymerase II (44), and DNA polymerase I (Klenow) (45), which have been reported to be 30, 72, 13, 20, and 50/s, respectively. Unlike the k_{cat} values, the values of K_m were independent of the length of RNA (N), and the average value of the seven RNAs was 2.9 ± 1.6 nM.

Analysis of the Saturation Point—The saturation point was analyzed to obtain α, n, and K_{m2} ($= (k_{-2} + 2k_{cat})/k_2$) values. At the saturation point, the concentration of RNA reaches that of working enzyme, and few enzyme molecules remain free (23). More precisely, since the affinity between the RNA and enzyme is sufficiently high (K_m values were on the order of 1 nM in Table 1), the RNA concentration at this point ([R_{sat}]) is equivalent to the concentration of working enzyme (*i.e.* the enzyme bound to the productive binding site of RNA ([*E*-Rp])). By using [R_{sat}], we are thus able to determine the concentration of working enzyme ([*E*-Rp]). In Fig. 2*A*, the saturation point and the RNA concentration at this point ([R_{sat}]) in a reaction is depicted for the reaction using 400 nM enzyme. The method to determine

TABLE 1
Experimentally determined kinetic parameters of seven different RNAs

Template RNA	N	k_{cat}[a]	K_m[a,b]	n[c]	K_{m2}[b,c]	$V_{cor}(0)$[d]	$V_{cor}(\infty)$[d]	K_i[d]
	nt	/min	nM		nM	nM/min	nM/min	nM
S130	130	3.6 ± 0.1	1.7 ± 0.3	ND[e]	ND	6.2 ± 0.2	5.8 ± 0.03	19.3 ± 13.8
S222	222	2.6 ± 0.08	1.0 ± 0.3	ND	ND	4.1 ± 0.3	2.4 ± 0.3	1.3 ± 0.1
MDV-poly	244	2.2 ± 0.07	4.2 ± 0.6	0.4 ± 0.2	5.3 ± 10.0	2.9 ± 0.5	1.9 ± 0.2	7.7 ± 2.3
MDV-T12	271	2.0 ± 0.03	2.6 ± 0.2	1.6 ± 0.8	59.2 ± 45.2	3.2 ± 0.4	1.8 ± 0.1	3.8 ± 1.6
MDV-CAT	936	1.2 ± 0.04	4.9 ± 0.7	3.0 ± 0.4	8.3 ± 2.2	1.4 ± 0.2	0.33 ± 0.07	6.0 ± 2.4
MDV-dBETA	1028	1.2 ± 0.05	4.1 ± 0.7	3.2 ± 1.1	29.6 ± 15.7	1.2 ± 0.1	0.38 ± 0.06	7.8 ± 2.0
MDV-BETA	2085	0.67 ± 0.02	1.2 ± 0.3	8.5 ± 5.0	49.6 ± 36.5	1.8 ± 0.2	0.55 ± 0.04	4.4 ± 0.1

[a] Determined by analysis of the exponential phase.
[b] Determined using the value $\alpha = 0.2$, obtained by analysis of the saturation point.
[c] Determined by analysis of the saturation point.
[d] Determined by analysis of the linear phase.
[e] ND, not determined.

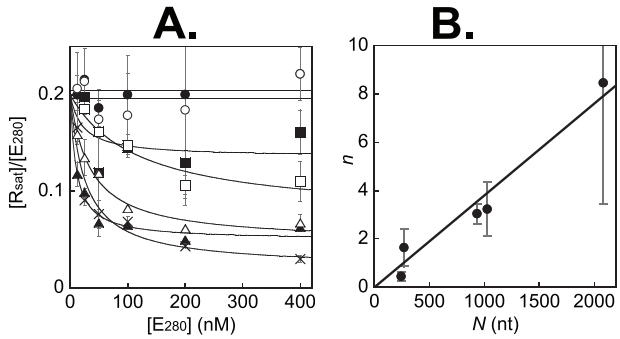

FIGURE 3. **Analysis of the saturation point.** $[R_{sat}]$ was determined as described under "Experimental Procedures." *A*, $[R_{sat}]/[E_{280}]$ as a function of $[E_{280}]$ for the following seven RNAs: S130 (●), S222 (○), MDV-poly (■), MDV-T12 (□), MDV-CAT (▲), MDV-dBETA (△), and MDV-BETA (×). The *solid lines* represent the fit of the data to Equation 9, which gave n and K_{m2}/α values shown in Table 1. *B*, the correlation between n and N. The *solid line* represents the linear regression of the data that gave a slope of 0.0038/nt, which indicates the average number of nonproductive binding sites on a single nucleotide of RNA.

$[R_{sat}]$ from the experimental results is described under "Experimental Procedures."

Based on Scheme 1, $[R_{sat}]/[E_{280}]$, which is the fraction of working enzyme at the saturation point, can be written as Equation 9 (see "Experimental Procedures"). K_{m2} is $(k_{-2} + 2k_{cat})/k_2$, which is the Michaelis-Menten-like constant between the enzyme and the nonproductive binding sites of the template RNA, not per molecule but per site. The $[R_{sat}]$ values for each of the seven RNAs at different enzyme concentrations were obtained from the same data used for analysis of the exponential phase. Fig. 3*A* shows the relationship between $[R_{sat}]/[E_{280}]$ and $[E_{280}]$ for the seven RNAs. The results indicated that longer RNAs show reduced values of $[R_{sat}]/[E_{280}]$ at increasing $[E_{280}]$, indicating that the fractions of working enzyme with longer RNAs are less than those of shorter RNAs at the saturation point. For two RNAs, S130 and S222 RNA, $[R_{sat}]/[E_{280}]$ values were not significantly different with varying $[E_{280}]$, which indicates that either K_{m2}/α was $\gg(1 + n)\cdot[E_{280}]$ or $n = 0$ (Equation 9) was true for these two RNAs. In both cases, $[R_{sat}]/[E_{280}]$ can be approximated to α (*i.e.* $[R_{sat}]/[E_{280}] = \alpha$). We thus obtained $\alpha = 0.20$, which is the average of α obtained for S130 and S222. In addition, since we did not see the dependence of $[R_{sat}]/[E_{280}]$ on the value of $[E_{280}]$, K_{m2} and n values of these two RNAs were not detectable (Table 1). Using this value, we then determined K_{m2} and n for the other five RNAs by fitting the data to Equation 9 (Fig. 3*A*, Table 1). From the results, we found that the values of n were in direct proportion to the length of the template RNA (N) and obtained the relationship $n = 0.0038N$ (Fig. 3*B*). This indicates that the template RNA has an average of one nonproductive binding site per 263 nt. Moreover, the observation that longer RNAs show reduced values of $[R_{sat}]/[E_{280}]$ at increasing concentrations of $[E_{280}]$ can be explained well by the presence of more nonproductive binding sites on these longer RNAs. Although the values of K_{m2} have substantial margins of S.E., we did not observe their dependence on the length of RNA, and the average value for the five RNAs was 30 ± 23 nM (Table 1).

Analysis of the Linear Phase —The linear phase was analyzed to obtain K_i ($= k_{-2}/k_2$) values and to evaluate the consistency of our results. For the analysis, the reactions were carried out using template RNA concentrations higher than those of the enzymes. Under such conditions, the reaction begins immediately from the linear phase (*i.e.* the RNA is present in excess relative to the enzyme throughout the reaction). During the linear phase, the enzyme concentration is rate-limiting, and the reaction velocity is proportional to the working enzyme concentration. Indeed, the initial velocity was directly proportional to the input enzyme concentration in the reaction started immediately from the linear phase (not shown). Hence, by measuring the reaction velocity, it is possible to trace the changes in the working enzyme concentrations, which allowed us to estimate the K_i values.

The *black dashed line* in Fig. 4*A* shows the time course of the RNA amplification initiated by 100 nM S222 RNA and 10 nM enzyme, and the *closed circles* show the time course of the reaction velocity on a logarithmic scale. In the reaction velocity ($V(t)$, *closed circles*), a single exponential decrease (linear line on a logarithmic scale) at the late stage and the deviation from the single exponential decrease at the early stage can be seen (Fig. 4*A*). The single exponential decrease and the deviation from it are considered due to enzyme inactivation and nonproductive binding of the enzyme, respectively. Under such assumptions, the reaction velocity at reaction time t ($V(t)$) can be written as Equation 14 (see "Experimental Procedures"). k_{inact} is the rate of enzyme inactivation, and K_i is k_{-2}/k_2, which is the dissociation constant between the enzyme and the nonproductive binding sites of the template RNA, not per molecule but per site. Equation 14 provided a good fit to the data (Fig. 4*A*, *black solid line*), indicating the validity of the proposed model and the assumptions used. In addition, as a result of the fit we obtained, $k_{inact} = 0.012 \pm 0.002$/min. This value was in agreement with

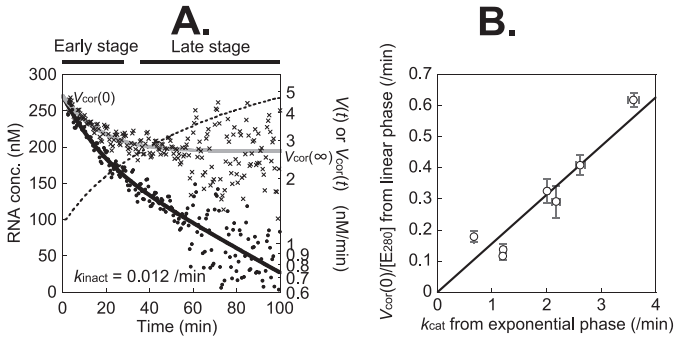

FIGURE 4. **Analysis of the linear phase.** *A*, the time course of changes in the RNA concentration (*left axis*, *black dashed line*), the reaction velocity ($V(t)$) (*right axis*, ●), and the corrected velocity ($V_{cor}(t)$) (*right axis*, ×) of the reaction using 100 nM S222 RNA and the enzyme at 10 nM. The *black solid line* represents the fit of the data to Equation 14, which gave $k_{cat}\cdot\alpha$, $n\cdot k_2\cdot K_m$, k_{-2}, and k_{inact} of 0.48 ± 0.02/min, 0.030 ± 0.005/min, 0.036 ± 0.012/min, and 0.012 ± 0.002/min, respectively. The *gray solid line* represents the corrected *black solid line* (Equation 13). *B*, the correlation between $V_{cor}(0)/[E_{280}]$ and k_{cat} values of seven different RNAs obtained by analysis of the linear and exponential phases, respectively. The *solid line* represents the fit of the data to a line that gave $\alpha = 0.16$, which is in agreement with the value of $\alpha = 0.20$ determined by analysis of the saturation point, suggesting the validity of our reaction model.

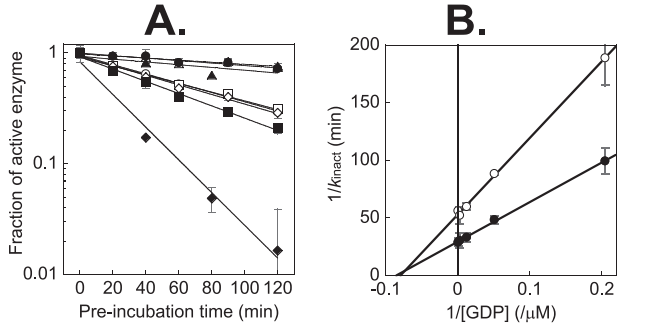

FIGURE 5. **Inactivation of Qβ replicase.** *A*, inactivation curves in the presence of different nucleotides: none (●); UTP, CTP, and GTP (○); ATP, CTP, and GTP (□); ATP, UTP, and GTP (◇); ATP, UTP, and CTP (△); GTP (■); GDP (◆), and GMP (▲). The concentrations of each nucleotide were 1.25 mM. The *solid lines* represent the fit of the data to a single exponential that gave the inactivation rate summarized in Table 2. *B*, Lineweaver-Burk plot of the inactivation rates as a function of GDP concentration without NTP (●) and in the presence of ATP, UTP, and CTP at 1.25 mM each (○). The *solid lines* represent the linear regression curves of the data, which gave the $k_{inactmax}$, $K_{m(GDP)}$, and $K_{i(NTP)}$ values as described under "Results."

that obtained independently with different experiments shown in Fig. 5*A* (see below for details). Moreover, since the rates of the single exponential decrease at the late stage (Fig. 4*A*) were independent of both enzyme and RNA concentrations (not shown), the decrease is likely to correspond to the enzyme inactivation.

The fit of $V(t)$ (Fig. 4*A*, *closed circles*) with Equation 14 can give the rate constants $k_{cat}\cdot\alpha$, $n\cdot k_2\cdot K_m$, k_{-2}, and k_{inact} of all seven different RNAs and in turn the K_i values ($K_i = k_{-2}/k_2$), using the values of n and K_m. However, for those exhibiting low amplification efficiency, in particular the reaction with longer RNAs, the errors of the real time data were large and insufficient for directly fitting with Equation 14 (for details, see "Experimental Procedures"). Therefore, we adopted another strategy to obtain the K_i values for all seven RNAs. First, the effect of enzyme inactivation was removed from $V(t)$ by using $k_{inact} = 0.012$/min, which gave $V_{cor}(t)$ (Fig. 4*A*, ×; see Equations 13 and 14). Here, the values of $V_{cor}(t)$ at the initial ($V_{cor}(0)$) and at the steady state ($V_{cor}(\infty)$; *i.e.* at the late stage) can be written as $k_{cat}\cdot\alpha\cdot[E_{280}]$ and $k_{cat}\cdot\alpha\cdot[E_{280}]/(n\cdot K_m/K_i + 1)$, respectively (see Equation 13), which then gave $K_i = n\cdot K_m/(V_{cor}(0)/V_{cor}(\infty) - 1)$. Therefore, by measuring the values of $V_{cor}(0)$ and $V_{cor}(\infty)$ for the seven RNAs that could be determined with reasonable accuracy (see "Experimental Procedures") and by using the K_m values determined by analysis of the exponential phase and using the relationship $n = 0.0038N$ obtained by analysis of the saturation point, we were able to determine K_i values for seven RNAs (Table 1). We did not observe the dependence of K_i on the length of RNA, and the mean value of the seven RNAs was 5.4 ± 3.9 nM, which is of the same order of magnitude as the mean value of K_m and K_{m2} (2.9 ± 1.6 and 30 ± 23 nM, respectively) and the dissociation constants between RNA and Qβ replicase reported previously (21, 22).

In principle, the values of k_2 and k_{-2} can be determined as $k_2 = 2k_{cat}/(K_{m2} - K_i)$ and $k_{-2} = k_2\cdot K_i$, respectively. However, the values of K_{m2} have substantial margins of S.E. (Table 1), and thus the values could not be determined with accuracy. Nevertheless, from the average values of equilibrium constants, both values of k_2/nM/min and k_{-2}/min can be approximated to be on the order of 0.1. On the other hand, the k_1 value can be determined as $k_1 = (k_{-1} + k_{cat})/K_m > k_{cat}/K_m$. Although we have no means to estimate the k_{-1} value, k_1 can be estimated to be at least k_{cat}/K_m, which was on the order of 1/nM/min (Table 1). These estimations, $k_2 \approx 0.1$/nM/min and $k_1 > 1$/nM/min (the association of productive binding is much faster than that of nonproductive binding), can explain the observed decrease in velocity at the early stage of $V_{cor}(t)$, as described below. More precisely, the high velocity at the beginning of the reaction ($V_{cor}(0)$) can be explained by the major fraction of enzymes binding to the productive binding sites, since the association of productive binding is much faster than that of nonproductive binding (*i.e.* $k_1 \gg n\cdot k_2$). Subsequently, the enzymes also bind gradually to the nonproductive binding sites until reaching the steady state, in which the ratio of enzyme bound to productive and nonproductive binding sites becomes the ratio of their equilibrium constants (*i.e.* K_i/n and K_m, respectively). Therefore, the gradual decrease of $V_{cor}(t)$ (*i.e.* $V_{Cor}(0)$ to $V_{Cor}(\infty)$) was observed, and the K_i value was determined from the ratio of these two values.

Using the values obtained in the present study (Table 1), we also evaluated the validity of our reaction scheme by investigating the consistency of the data obtained by analysis of the linear phase with those of the exponential phase and the saturation point. The ratio of $V_{cor}(0)$ to $[E_{280}]$ can be written as $V_{cor}(0)/[E_{280}] = \alpha\cdot k_{cat}$, where $V_{cor}(0)/[E_{280}]$, and k_{cat} values were determined from the linear and exponential phases, respectively. A linear correlation was observed when plotting $V_{cor}(0)/[E_{280}]$ and k_{cat} for each RNA (Fig. 4*B*), which indicates the consistency between analysis of the linear and exponential phases. Furthermore, from the slope, the α value was determined to be 0.16, which was in agreement with the value of $\alpha = 0.20$ determined by analysis of the saturation point (Fig. 3*A*). The fact that the values obtained from three different experiments obeyed one equation suggests the consistency of our analysis and further justifies our model.

TABLE 2
Inactivation rates in the presence of different nucleotides obtained in Fig. 5*A*

Additives	Inactivation rate
	10^{-2}/min
None	0.26 ± 0.09
UTP, CTP, and GTP	0.96 ± 0.04
CTP, GTP, and ATP	0.91 ± 0.02
GTP, ATP, and UTP	1.00 ± 0.08
ATP, UTP, and CTP	0.22 ± 0.04
GTP	1.28 ± 0.12
GDP	3.80 ± 0.35
GMP	0.26 ± 0.18

Analysis of the Enzyme Inactivation—We investigated whether the observed single exponential decrease in the velocity in the linear phase is indeed due to enzyme inactivation. Qβ replicase is known to be stable under cell-free conditions (3). On the other hand, the presence of guanine nucleotides has been reported to accelerate the inactivation (46). Therefore, we determined the inactivation rate in the presence of GTP, which is present in the replication reaction, and also examined the effects of other guanine nucleotides (GDP and GMP).

The inactivation rate was determined from the decreasing fraction of the active enzyme by preincubation of the enzyme. The fraction of the active enzyme was determined from the initial velocity of the reaction initiated from the linear phase, which was directly proportional to the enzyme concentration (not shown), after preincubation. We first determined the inactivation rates under the same conditions as for the replication reaction except that one or all four NTPs were omitted. Fig. 5*A* shows the time course of enzyme inactivation on a logarithmic scale, and the inactivation rates are summarized in Table 2. These results indicated that the inactivation rate is roughly 0.01/min as long as GTP is present, which is in agreement with that shown in Fig. 4*A* (0.012 ± 0.002/min). The observation that the inactivation rate determined from the reaction (Fig. 4*A*) was slightly greater than that determined from the preincubation experiments (Fig. 5*A*) may be due not only to experimental error but also to the presence of another inactivation mechanism, such as polymerase arrest (47). On the other hand, the inactivation rates in the absence of GTP were significantly slower than that in the presence of GTP (roughly 0.002/min). In addition, GDP was found to accelerate the rate to 0.038/min, whereas GMP did not (Fig. 5*A*, Table 2). These results were in good agreement with those of a previous study, where the rate constants were not determined but the effects of GTP and GDP were shown qualitatively (46).

The inactivation with GDP was significantly faster than that with GTP. Therefore, we performed further investigations of the GDP-dependent inactivation. Previously, GDP-dependent inactivation was reported to be due to the binding of GDP to the EF-Tu subunit of Qβ replicase (46). On the other hand, the β subunit, which catalyzes elongation, binds to NTPs. Therefore, we investigated the influence of NTP on the GDP-dependent inactivation by incubating the enzyme in the presence of three NTPs at 1.25 mM (each of ATP, CTP, and UTP) and various concentrations of GDP. Fig. 5*B* shows the Lineweaver-Burk plot of the results, which indicated that NTPs seem to inhibit the GDP-dependent inactivation in a noncompetitive manner. In addition, the maximum inactivation rate ($k_{inactmax}$), the Michaelis-Menten constant of the GDP-dependent inactivation ($K_{m(GDP)}$), and the inhibition constants ($K_{i(NTP)}$; *i.e.* dissociation constant of the inactivation inhibition by NTP) averaged for ATP, CTP, and UTP were determined to be 0.034/min, 12 μM, and 4.7 mM, respectively. Similarly, we also determined $K_{i(NTP)}$ for each of the four NTPs to be 15.2 ± 0.2, 8.3 ± 0.1, 3.6 ± 0.3, and 5.5 ± 0.1 mM for ATP, UTP, CTP, and GTP, respectively, which indicated that all of the NTPs (including GTP) inhibited the GDP-dependent inactivation with little difference in magnitude between the nucleotide bases. Although the molecular mechanism has yet to be determined, it is clear that the stability of Qβ replicase can be regulated by the concentrations of both NTPs (on the order of 1 mM in *Escherichia coli* (48)) and GDP. The balance of NTP and GDP concentrations may be used as a regulatory mechanism for Qβ phage infection and amplification.

DISCUSSION

In this study, we analyzed the entire process of RNA amplification by Qβ replicase based on a simple kinetic model, which considers nonproductive binding. Our study revealed that the model was capable of explaining the results obtained throughout the entire process: exponential phase, saturation point, and linear phase. Our model can also explain three previously unresolved observations. First, the replication of the phage genomic RNA was shown to be inhibited somehow by the genomic RNA itself (26, 27), and the inhibition did not depend on either the enzyme or the genomic RNA concentration but on the ratio of the enzyme to RNA. This observation can be explained as competitive inhibition by nonproductive binding, where the affinity of nonproductive binding is higher than that of productive binding (*i.e.* K_i/n is smaller than K_m), which is probably the case for long RNAs, such as the genomic RNA. Second, the reaction velocity decreases in the linear phase (5, 28), which has been explained as an effect of uncompetitive inhibition by the template RNA (11). In the case of uncompetitive inhibition, the reaction velocity should depend on the RNA concentration. However, we found that the decrease in velocity was independent of the RNA concentration (not shown), which was also the case for genome amplification described above (26, 27). In our model, this observation can be explained as the decrease in the working enzyme caused by both nonproductive binding and enzyme inactivation. Third, the catalytic constant (k_{cat}) has been reported to differ between the exponential and linear phases. This observation was based on the assumption that the entire enzyme molecule is working (*i.e.* $\alpha = 1$) (5), which is obviously inappropriate and should cause overestimation of the working enzyme concentration. In the linear phase, the velocity is proportional to the enzyme concentration, as described under "Results," and overestimation of the enzyme concentration leads to underestimation of k_{cat}. On the other hand, k_{cat} can be obtained independently of the enzyme concentration in the exponential phase, and as a consequence k_{cat} values were thought to be different between the two phases.

Alternatively, based on our results, it is more reasonable that $\alpha \neq 1$, and k_{cat} is constant throughout the reaction.

In addition to the kinetic model, we obtained various kinetic constants of the replication reaction for RNAs of varying length (Table 1). We also found a correlation between the inverse of catalytic constant ($1/k_{cat}$) and the length of template RNA (N) (Fig. 2*C*) and a correlation between the number of nonproductive binding sites on a single template RNA (n) and N (Fig. 3*B*), which allows estimation of k_{cat} and n values from the value of N. These values represent important information both for understanding the basis of Qβ phage amplification and for applications using Qβ replicase. Using our estimate, the catalytic rate of the Qβ phage genome (4217 nt) replication can be predicted to be 0.006/s, which is also in agreement with the value 0.01/s obtained by simulations reported previously (14, 49). By knowing the correlation between n and N ($n = 0.0038N$; Fig. 3*B*), we can designate the two effects caused by nonproductive binding as described below. First, the exponential phase should be shorter for the longer RNA. More precisely, the RNA amplification comes to the end of the exponential phase (*i.e.* saturation point) when the RNA concentration is equal to the working enzyme concentration (*i.e.* $[R_{sat}] \approx [Et]/(1 + n)$; see Equation 9). Second, the affinity of nonproductive binding should become greater for longer RNA, which causes a significant decrease of the reaction velocity in the linear phase. More precisely, the dissociation constant of nonproductive binding for a single RNA molecule is K_i/n, which becomes smaller for longer RNAs. These estimations suggest the difficulty of Qβ phage genome amplification *in vivo*, which is 4127 nt in length, even longer than all seven RNAs used in the present study.

Nonproductive binding should exhibit a substantial effect during genome amplification *in vivo*, since nonproductive binding is more effective for longer RNAs that carry larger numbers of nonproductive binding sites. Furthermore, the host *E. coli* cell is filled with other RNAs, such as rRNA, tRNA, mRNA, *etc.*, which will inhibit genome amplification competitively by nonproductive binding. Despite the many difficulties, the Qβ phage genome can indeed be amplified *in vivo*. Based on our results, we suggest that the faster association of the enzyme to productive than to nonproductive binding sites is one of the keys enabling phage genome replication *in vivo*. Moreover, the slower association of nonproductive binding may be used as a regulatory mechanism of the life cycle of the phage. For example, the inactivation of the Qβ replicase by nonproductive binding may be necessary for suppression of the amplification of parasite RNA (called 6 S RNA (3)) after the genome amplification reaction. Alternatively, nonproductive binding may maintain the genomic RNA in a single-stranded form, necessary for the RNA amplification and translation reactions. Clearly, further studies are required to understand the role of nonproductive binding *in vivo*.

The mechanism of synthesizing the minus strand of the Qβ phage genome using the plus strand as a template is rather complex (50). Subunit S1 and another host factor, Hfq protein, are necessary for this reaction, whereas these are not necessary for replication of all other known amplifiable RNAs, including synthesis of the plus strand of the genome from the minus strand (51). In the present study, we used S1-less Qβ replicase (see "Experimental Procedures"), a different form from that *in vivo*. Nevertheless, nonproductive binding should be present with the replicase *in vivo*, because holoenzyme (with S1) is also known to bind various RNAs, regardless of whether the RNA is amplifiable or not (4, 22), and the Hfq protein only mediated access of the replicase to the 3′-end of the plus strand of the phage genome (52).

Competitive inhibition by nonproductive binding (also known as nonspecific binding (38, 53)) is known for other enzymes (35), whereas it has not been reported previously for Qβ replicase. The mechanism responsible for the number of nonproductive binding sites (n) being proportional to the length of RNA (N) is unclear ($n = 0.0038N$; Fig. 3*B*). However, there are two possibilities. First, the nonproductive binding sites on the RNA are pyrimidine tracts, which may be distributed evenly on the RNA. Qβ replicase is known to possess two different RNA binding sites (binding sites I and II), and binding site II, which is located on the EF-Tu subunit (4) is known to bind pyrimidine tracts preferentially (22). The dissociation constant of binding between replicase and polypyrimidine (7 and 20 nt) was found to be in the range of 1–10 nM (22), which was similar to that of the nonproductive binding (K_i) in our results (5.4 nM on average (Table 1)). When we investigated the number of heptapyrimidine sequences (n_{seq}) within both the plus and the minus strands of the five RNA sequences used in this study and compared n_{seq} and n, we observed a linear correlation with a slope of 0.94 ($R^2 = 0.77$), suggesting that the heptapyrimidine sequence may be the nonproductive binding site. It should be noted, however, that this was not the case with the number of hexa- or octapyrimidine sequences, and thus heptapyrimidine may have a particular role in binding to the replicase. Alternatively, n may simply be determined by steric hindrance due to the binding of a number of replicase molecules on the RNA of limited length. We found that one molecule of Qβ replicase can bind per 263 nt of RNA on average ($n = 0.0038N$; Fig. 3*B*), corresponding to a single replicase on ~90 nm of stretched RNA (54). RNA does not exist in a stretched form but generally folds to a much more compact topology, and thus 263-nt RNA should be much smaller than 90 nm. The diameter of the EF-Tu and Ts complex is ~10 nm (55), and thus Qβ replicase is likely to be slightly larger than 10 nm. The correlation $n = 0.0038N$ can be understood if the length of 263-nt RNA is in a range similar to the size of the replicase. Note that if $n = 0.0038N$ is determined by the steric hindrance, the number n (and consequently the value 0.0038) obtained in this study may be underestimated because of the difficulty of forming a close packed state (*i.e.* RNA saturated with the replicase without any distance between the enzymes), as described previously by McGhee *et al.* (56). Further studies are required to determine the detailed molecular mechanism of nonproductive binding.

We assumed that nonproductive binding does not inhibit elongation of other enzyme molecules on the same template RNA and does not affect the value of k_{cat}. This assumption was justified by the experimental data, as described below. In the exponential phase, the fraction of the enzyme bound to the nonproductive binding site of RNA (E-Rn) increased as with the increase of enzyme concentration following Equa-

tion 8 (Fig. 3*A*). If nonproductive binding inhibits elongation, the rate of exponential amplification (k_{obs}) should decrease with the increase of enzyme concentration; however, k_{obs} did not decrease in the experiment (Fig. 2*B*). Therefore, the inhibition of elongation by nonproductive binding was not observed, and even if present, the effect is significantly small and negligible.

The aim of this study was to interpret the RNA amplification process as simply as possible. Therefore, we did not consider asymmetry of the RNA strands (25) and the production of double-stranded RNA (23), which are known to be present. Indeed, we observed differences in kinetic constants between the plus and minus strand of some RNAs and the production of double-stranded RNA, which can no longer act as a template (not shown). We ignored the asymmetry, and thus our estimates can be interpreted as the averages of two complementary strands. Double-stranded RNA production is a reaction in which newly synthesized RNA anneals fully with the template RNA at the end of the polymerization reaction. It has been reported that the ratio of double-stranded RNA production depends on the structure of the RNA (24), and the ratio affects the rate of exponential amplification of RNA (k_{obs}) (57). Therefore, the values of k_{cat} (consequently k_{pol} and k_{others}) and α obtained in the present study can be affected by considering double-stranded RNA production. Following the previous report (57), when considering double-stranded RNA production, the values of k_{cat} and α can be corrected as $k_{cat}/(1 - 2d)$ and $\alpha \cdot (1 - 2d)$, respectively, where d represents the ratio of double-stranded RNA production. The value of d can be obtained as the ratio of double-stranded RNA to total RNA, assuming that the double-stranded RNA is produced only by newly synthesized RNA with the template RNA at the end of elongation and not by the annealing of two free complementary strands. We measured the values of d by gel electrophoresis for all seven RNAs used in this study, and all were in the range of 0.2–0.3 with little difference among the RNAs (not shown). Therefore, all values of k_{cat} and α may be under- and overestimated by at most ~2-fold, respectively. Note that d values obtained in the present study may be overestimated, since we were not able to distinguish double-stranded RNA production during the reaction and gel electrophoresis. Hence, the degree of overestimation of k_{cat} and α is less than 2-fold. Nevertheless, it is worth noting that the relationships between $1/k_{cat}$ and N (Fig. 2*C*), $V_{cor}(0)/[E_{280}]$ and k_{cat} (Fig. 4*B*), and α and the slope of the line in Fig. 4*B* are unaffected regardless of the presence or absence of double-stranded RNA.

In conclusion, we have proposed a plausible kinetic model for the RNA replication reaction by Qβ replicase and determined the various kinetic constants. This study provides new insight into the biology of Qβ phage, such as the effect of nonproductive binding and the notable pattern of enzyme inactivation, and also provides useful information for applications using Qβ replicase, such as estimation of the catalytic constant and the number of nonproductive binding sites from the length of the template RNA and the ranges of the various equilibrium constants. Further studies, such as determination of the three-dimensional structure (58, 59) of Qβ replicase, would be helpful in extending our understanding of the molecular mechanism of action of this enzyme.

Acknowledgments—We thank Dr. Inokuchi Yoshio for the gift of plasmid pUC-MDV-LR. We are also grateful to Drs. Itaru Urabe, Akiko Kashiwagi, and Yasufumi Shima for helpful discussion and Ichiro Taniguchi for preparation of Qβ replicase.

REFERENCES

1. Calendar, R. (2006) *The Bacteriophages*, 2nd Ed., pp. 175–196, Oxford University Press, Oxford
2. Haruna, I., and Spiegelman, S. (1965) *Proc. Natl. Acad. Sci. U. S. A.* **54,** 579–587
3. Chetverin, A. B., and Spirin, A. S. (1995) *Prog. Nucleic Acids Res. Mol. Biol.* **51,** 225–270
4. Brown, D., and Gold, L. (1996) *Proc. Natl. Acad. Sci. U. S. A.* **93,** 11558–11562
5. Biebricher, C. K., Eigen, M., and Luce, R. (1981) *J. Mol. Biol.* **148,** 391–410
6. Yoshinari, S., and Dreher, T. W. (2000) *Virology* **271,** 363–370
7. Tretheway, D. M., Yoshinari, S., and Dreher, T. W. (2001) *J. Virol.* **75,** 11373–11383
8. Brown, D., and Gold, L. (1995) *Biochemistry* **34,** 14775–14782
9. Zamora, H., Luce, R., and Biebricher, C. K. (1995) *Biochemistry* **34,** 1261–1266
10. Ugarov, V. I., Demidenko, A. A., and Chetverin, A. B. (2003) *J. Biol. Chem.* **278,** 44139–44146
11. Biebricher, C. K., Eigen, M., and Gardiner, W. C., Jr. (1983) *Biochemistry* **22,** 2544–2559
12. Chetverin, A. B., Chetverina, H. V., Demidenko, A. A., and Ugarov, V. I. (1997) *Cell* **88,** 503–513
13. Mills, D. R., Peterson, R. L., and Spiegelman, S. (1967) *Proc. Natl. Acad. Sci. U. S. A.* **58,** 217–224
14. Eigen, M., Biebricher, C. K., Gebinoga, M., and Gardiner, W. C. (1991) *Biochemistry* **30,** 11005–11018
15. Biebricher, C. K., Eigen, M., and Luce, R. (1986) *Nature* **321,** 89–91
16. Morozov, I. Y., Ugarov, V. I., Chetverin, A. B., and Spirin, A. S. (1993) *Proc. Natl. Acad. Sci. U. S. A.* **90,** 9325–9329
17. Abramson, R. D., and Myers, T. W. (1993) *Curr. Opin. Biotechnol.* **4,** 41–47
18. Tyagi, S., Landegren, U., Tazi, M., Lizardi, P. M., and Kramer, F. R. (1996) *Proc. Natl. Acad. Sci. U. S. A.* **93,** 5395–5400
19. Mills, D. R., and Kramer, F. R. (1979) *Proc. Natl. Acad. Sci. U. S. A.* **76,** 2232–2235
20. Kopsidas, G., Roberts, A. S., Coia, G., Streltsov, V. A., and Nuttall, S. D. (2006) *Immunol. Lett.* **107,** 163–168
21. Werner, M. (1991) *Biochemistry* **30,** 5832–5838
22. Preuss, R., Dapprich, J., and Walter, N. G. (1997) *J. Mol. Biol.* **273,** 600–613
23. Priano, C., Kramer, F. R., and Mills, D. R. (1987) *Cold Spring Harb. Symp. Quant. Biol.* **52,** 321–330
24. Axelrod, V. D., Brown, E., Priano, C., and Mills, D. R. (1991) *Virology* **184,** 595–608
25. Biebricher, C. K., Eigen, M., and Gardiner, W. C., Jr. (1984) *Biochemistry* **23,** 3186–3194
26. Kondo, M., and Weissmann, C. (1972) *Eur. J. Biochem.* **24,** 530–537
27. Inokuchi, Y., and Kajitani, M. (1997) *J. Biol. Chem.* **272,** 15339–15345
28. Palmenberg, A., and Kaesberg, P. (1974) *Proc. Natl. Acad. Sci. U. S. A.* **71,** 1371–1375
29. Nakaishi, T., Iio, K., Yamamoto, K., Urabe, I., and Yomo, T. (2002) *J. Biosci. Bioeng.* **93,** 322–327
30. Kita, H., Cho, J., Matsuura, T., Nakaishi, T., Taniguchi, I., Ichikawa, T., Shima, Y., Urabe, I., and Yomo, T. (2006) *J. Biosci. Bioeng.* **101,** 421–426
31. Inokuchi, Y., Kajitani, M., and Hirashima, A. (1994) *J. Biochem.* (*Tokyo*) **116,** 1275–1280
32. Lizardi, P. M., Guerra, C. E., Lomeli, H., Tussie-Luna, I., and Russell Kramer, F. (1988) *Bio/Technology* **6,** 1197–1202

33. Chetverin, A. B., Chetverina, H. V., and Munishkin, A. V. (1991) *J. Mol. Biol.* **222,** 3–9
34. Knuth, D. E. (1992) *Am. Math. Mon.* **99,** 403–422
35. Fersht, A. (1999) *Structure and Mechanism in Protein Science: A Guide to Enzyme Catalysis and Protein Folding*, pp. 114–116, W.H. Freeman, New York
36. Thoma, J. A., and Koshland, D. E. (1960) *J. Am. Chem. Soc.* **82,** 3329–3333
37. Lin, S. Y., and Riggs, A. D. (1970) *Nature* **228,** 1184–1186
38. Langowski, J., Pingoud, A., Goppelt, M., and Maass, G. (1980) *Nucleic Acids Res.* **8,** 4727–4736
39. Kacian, D. L., Mills, D. R., Kramer, F. R., and Spiegelman, S. (1972) *Proc. Natl. Acad. Sci. U. S. A.* **69,** 3038–3042
40. Mills, D. R., Dobkin, C., and Kramer, F. R. (1978) *Cell* **15,** 541–550
41. Jia, Y., and Patel, S. S. (1997) *Biochemistry* **36,** 4223–4232
42. Arnold, J. J., and Cameron, C. E. (2000) *J. Biol. Chem.* **275,** 5329–5336
43. Lanchy, J. M., Ehresmann, C., Le Grice, S. F., Ehresmann, B., and Marquet, R. (1996) *EMBO J.* **15,** 7178–7187
44. Narayan, S., Widen, S. G., Beard, W. A., and Wilson, S. H. (1994) *J. Biol. Chem.* **269,** 12755–12763
45. Kuchta, R. D., Mizrahi, V., Benkovic, P. A., Johnson, K. A., and Benkovic, S. J. (1987) *Biochemistry* **26,** 8410–8417
46. Blumenthal, T. (1977) *Biochim. Biophys. Acta* **478,** 201–208
47. Susa, M., Sen, R., and Shimamoto, N. (2002) *J. Biol. Chem.* **277,** 15407–15412
48. Albe, K. R., Butler, M. H., and Wright, B. E. (1990) *J. Theor. Biol.* **143,** 163–195
49. Kim, H., and Yin, J. (2004) *Biotechnol. Bioeng.* **88,** 148–156
50. Klovins, J., Berzins, V., and van Duin, J. (1998) *RNA* **4,** 948–957
51. Blumenthal, T., and Carmichael, G. G. (1979) *Annu. Rev. Biochem.* **48,** 525–548
52. Schuppli, D., Miranda, G., Tsui, H. C., Winkler, M. E., Sogo, J. M., and Weber, H. (1997) *Proc. Natl. Acad. Sci. U. S. A.* **94,** 10239–10242
53. von Hippel, P. H., Revzin, A., Gross, C. A., and Wang, A. C. (1974) *Proc. Natl. Acad. Sci. U. S. A.* **71,** 4808–4812
54. Alberts, B. (2002) *Molecular Biology of the Cell*, 4th Ed., pp. 191–374, Garland Science, New York
55. Kawashima, T., Berthet-Colominas, C., Wulff, M., Cusack, S., and Leberman, R. (1996) *Nature* **379,** 511–518
56. McGhee, J. D., and von Hippel, P. H. (1974) *J. Mol. Biol.* **86,** 469–489
57. Davis, B. K. (1995) *Philos. Trans. R. Soc. Lond. B Biol. Sci.* **350,** 345–352
58. Messias, A. C., and Sattler, M. (2004) *Acc. Chem. Res.* **37,** 279–287
59. Ortin, J., and Parra, F. (2006) *Annu. Rev. Microbiol.* **60,** 305–326